Universiteit Antwerpen

This item is the archived peer-reviewed author-version of:

A flexible low-cost biologically inspired sonar sensor platform for robotic applications

**Reference:**
Laurijssen Dennis, Kerstens Robin, Schouten Girmi, Daems Walter, Steckel Jan.- A flexible low-cost biologically inspired sonar sensor platform for robotic applications IEEE international conference on robotics and automation / IEEE International Conference on Robotics and Automation; Institute of Electrical and Electronics Engineers, Computer Society - ISSN 2577-087X - New york, Ieee, (2019), p. 9617-9623
Full text (Publisher's DOI): https://doi.org/10.1109/ICRA.2019.8794165
To cite this reference: https://hdl.handle.net/10067/1651890151162165141

uantwerpen.be
Institutional repository IRUA

# A Flexible Low-Cost Biologically Inspired Sonar Sensor Platform for Robotic Applications

Dennis Laurijssen, Robin Kerstens, Girmi Schouten, Walter Daems & Jan Steckel

***Abstract*— In this paper we present a flexible low-cost sonar sensor platform that can be used for a wide range of biomimetic sonar experiments and autonomous sonar navigation targeted at robotics applications. The navigation abilities of bats using ultrasound (sonar) in unknown cluttered environments are very effective and can be distilled into a sensor architecture and accompanying control methodology that lends itself to be implemented on cost efficient hardware. The sensor architecture and processing methodology of this sensing platform mimics that of bats. In this paper we specifically focused on the common big-eared bat (*Micronycteris microtis*) although this could be transferred to other bat species or even other echolocating animals since the experimental platform was designed for flexibility. Using this platform we were able to implement a control system using a subsumption architecture that features different behavior patterns based solely on the sonar sensor as a source of exteroceptive information. In order to validate the combination of our autonomous navigation control system and our developed sonar sensor platform, the hardware was mounted on the P3DX robotics platform that was introduced in an unknown testing environment and have it drive autonomously. These experiments were used to validate our assumption of the efficacy of these relatively simple biomimetic control mechanisms and thus alleviating the need for expensive sensing platforms for certain robotics applications.**

## I. INTRODUCTION

One of the traits that defines the organisms in the animal kingdom is the ability to move. In addition, even creatures with only a limited amount of neurons are capable of navigation [1], [2]. Although the control mechanisms and sensor modalities used to navigate through unknown cluttered environments may differ between different animal species, these mechanics have proven their worth due to natural selection. An example of a relatively simple yet effective control mechanism can be found in bats and their use of ultrasound echolocation which has inspired us to create a flexible low-cost ultrasound (sonar) sensor experimentation platform. We condensed the sonar sensor modality of bats down to a broadband ultrasound speaker to mimic a bat's nose or mouth with ultrasound emitting capabilities combined with two small microphones that can be inserted into 3D-printed replicas of its ears for capturing the reflected ultrasound emissions [3], [4]. In this way we were able to create a small yet very powerful and flexible experimental platform which enables us to mimic the echolocating [5], [6] properties of different species of bats. The biomimetic approach in combination with ultrasonic pulse-echo sensing has proven to become a valid option for both navigation and Simultaneous Localization And Mapping [7]–[9]. To demonstrate our flexible low-cost sonar sensor platform we have looked into the behavior of the common big-eared bat (*Micronycteris microtis*) [10] of which an example can be seen in the right panel of Figure 1. Besides its characteristic ultrasonic call and using the 3D-printed replica of its ears, we have created a reactive control system [11] based on its navigational behaviour using a subsumption architecture [12]. This control system only makes use of sonar data in order to have the two-wheeled P3DX [13] robot navigate through its environment and establish the Sense-and-Avoid (SAA) functionality.

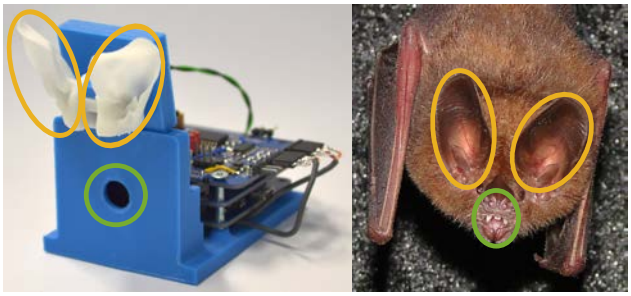

Fig. 1. On the left a photo of our proposed flexible sonar sensing platform which has been mounted on a 3D-printed fixture [14], which also serves as a baffle for our emitter, together with the replica of the common big-eared bat pinnae and a photo of the common big-eared bat (*Micronycteris microtis*) on the right courtesy of Inga Geipel. In both images the emission and reception sub-systems are marked

In order to perform experiments with the mobile robot with our novel sonar sensor platform and the reactive control architecture for validating our claims we have used a Hokuyo UBG-04LX-F01 LIDAR [15] to establish a ground truth for our test environment. Our ground truth is created using the Robot Operating System's (ROS) [16] GMapping functionality, which uses the FastSLAM 2.0 algorithm, that makes use of the aforementioned LIDAR. Once our reference map

Dennis Laurijssen is with the CoSys-Lab at the Faculty of Applied Engineering, University of Antwerp, Belgium, and with the Flanders Make Strategic Research Centre. (email: dennis.laurijssen@uantwerpen.be)

Robin Kerstens is with the CoSys-Lab at the Faculty of Applied Engineering, University of Antwerp, Belgium, and with the Flanders Make Strategic Research Centre. (email: robin.kerstens@uantwerpen.be)

Girmi Schouten is with the CoSys-Lab at the Faculty of Applied Engineering, University of Antwerp, Belgium, and with the Flanders Make Strategic Research Centre. He is also an SB PhD fellow at FWO (Research Foundation - Flanders), project [1S09417N]. (email: girmi.schouten@uantwerpen.be)

Walter Daems is with the CoSys-Lab at the Faculty of Applied Engineering, University of Antwerp, Belgium, and with the Flanders Make Strategic Research Centre. (email: walter.daems@uantwerpen.be)

Jan Steckel is with the CoSys-Lab at the Faculty of Applied Engineering, University of Antwerp, Belgium, and with the Flanders Make Strategic Research Centre. (email: jan.steckel@uantwerpen.be)

was created, the trajectory of the robot could be recorded throughout our autonomous driving experiments.

In the remainder of this paper, we will discuss the sensor architecture and its specific traits in the subsequent section, after which we will describe the signal processing techniques that are performed to establish the control architecture with its emergent behavioral patterns. The experimental results, that validate our proposed sensor platform, are described in Section V. In the final section, a brief discussion of these obtained experimental results, conclusion and future work will be presented.

## II. SENSOR ARCHITECTURE

In the last few years, increasingly more powerful ARM microcontrollers with low power consumption that feature a great variety of on-board peripherals have been introduced in a variety of product ranges at reasonable prices . The devices of the ARM Cortex M4 microcontroller product line are capable of having high clock speeds, relatively large RAM memory and a great number of on-board peripherals which made them very suitable for our sonar sensor platform. More specifically an STM32F429 Cortex M4 microcontroller was chosen at its core as can be seen in Figure 2.

For these biomimetic experiments we distinguish three different types of Printed Circuit Boards (PCBs): the core board that features our microcontroller, a USB communication board that enables USB data transfers for offloading data and an amplifier board that is used for driving the ultrasonic transducer and amplifying the microphone signals. The combination of these three printed circuits boards, as shown in Figure 3a, together with two small microphones and an ultrasonic transducer form our flexible sonar sensor platform. The two small microphones fit into the ear canals of the 3D-printed pinnae of the common big-eared bat. Since every individual board uses the same connector layout on both the top and bottom of the PCB, the system functionality can easily scale to other functionality or connectivity options depending on the specific application simply by stacking these PCBs. This feature contributes vastly to the flexible character of the sensor system.

### A. Core Board

As the main hub for our layered structure, the core board features the main microcontroller, the aforementioned STM32F429 [17] (as shown in Figure 3b). This microcontroller is programmed to set up its peripherals and allocate its memory for transmitting and receiving ultrasonic transmissions. After which it generates a logarithmic chirp signal ranging from 45 kHz to 20 kHz and finally initializes its state machine that controls the data acquisition flow. Using this state machine we are also able to reconfigure various parameters, e.g. the sampling frequencies, the transmission or reception length and start the transmission and reception actions which in their turn trigger data transmissions. In order to transmit and receive ultrasonic signals, the on-board 12-bit DAC peripheral is used to convert the calculated output

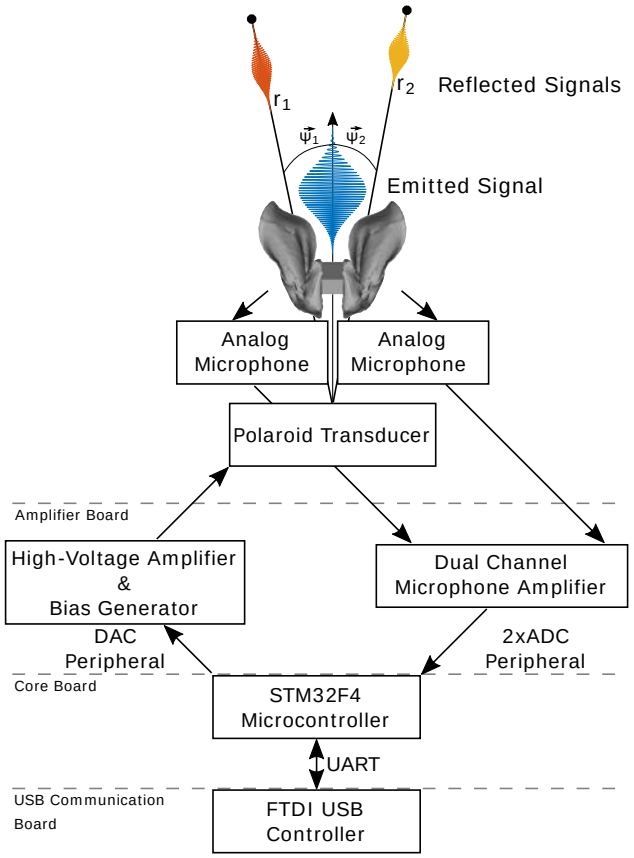


Fig. 2. Schematic hardware overview of the sonar sensor platform. The core the sensor platform features an ARM Cortex M4 microcontroller that uses its DAC peripheral to create the ultrasonic emitter signal and its two synchronous ADC peripherals to capture the microphone data of the reflected ultrasound emission. The microcontroller's UART peripheral is used for both offloading the microphone data to a computer and controlling the state machine. By using a specialized IC from FTDI the UART communication is converted to the nowadays standard USB 2.0 communication protocol.

signal values to an analog waveform. The two on-board synchronous 12-bit Analog-to-Digital Converter (ADC) peripherals are used to digitize the reflected ultrasound emissions captured by two small Knowles FG-23329 [18] microphones. By using connectors on both the top and bottom side of each board, these signals can be interconnected to other expansion boards.

### B. Amplifier Board

The ADC input and DAC output signals connect to the amplifier board, shown in Figure 3d. As the name suggests it features the amplification stage for the analog signals. On one end, two non-inverting op-amp amplifiers have been used to amplify the microphone signals to be fed to the ADC channels while the DAC waveform is amplified using a high-voltage amplifier in combination with a custom 150 V bias generator for driving a Senscomp 7000 Ultrasonic Transducer [19], which is commonly referred to as a Polaroid transducer.

### C. USB Communication Board

For offloading the microphone data to a (single-board) computer that further processes the data and controls the microcontroller's state machine, a USB 2.0 communication link has been chosen. A specialized IC from FTDI [20] performs the conversion to-and-from the USB interface to the microcontroller's UART peripheral at a stable $3\,\mathrm{Mbit/s}$. Since USB-communication with a host is not always required or could be replaced with a wireless alternative we have decided to place this layer on a separate USB communication PCB, shown in (Figure 3c), that also interconnects with the other printed circuit boards.

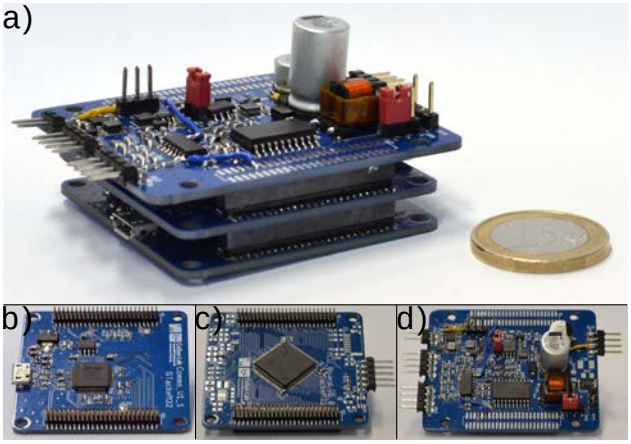


Fig. 3. Panel a depicts the stack of printed circuit boards that is used in our flexible sonar sensor platform. This setup measures $7.5\,\mathrm{cm x 5.0\,cm x 2.8\,cm}$. Panels b, c and d depict the individual PCBs that are used to form the stack.

### D. Sonar Sensor Platform

The proposed flexible low-cost sensor sonar platform thus comprises of the aforementioned printed circuits boards, two Knowles FG-23329 microphones and a Senscomp 7000 transducer that is baffled [14] with our 3D-printed fixture, which is shown on the left-hand side of Figure 1. This baffle features a tapered aperture, which reduces the aperture's size that in turn widens the directivity pattern of the transducer. While the fixture is printed using a nowadays common Fused Deposition Modeling (FDM) 3D-printer, the *Micronycteris microtis* pinnae replicas where fabricated using a stereolithography (SLA) 3D-printer. This process was chosen due to the complex shape and details of the pinnae that were unfeasible using the FDM printing technology.

In order to use this platform for the autonomous navigation of the P3DX robot, our hardware platform is connected to an Intel NUC computer that in turn is connected to the robot using a USB-to-serial cable. The computer will collect the data from the sonar sensor, perform the signal processing which will determine the behavior of the robot and send motor commands to the P3DX using ROS. This setup is shown in Figure 4c and as a block diagram in Figure 4b.

## III. SIGNAL PROCESSING

As mentioned earlier our chosen subsumption control architecture determines the behavior of the autonomous robot

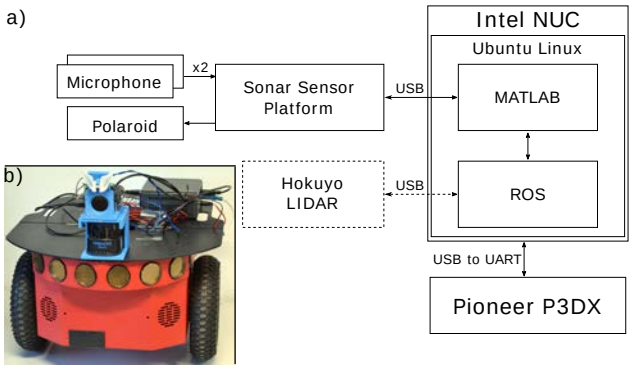


Fig. 4. Panel a shows the block diagram of the overall system setup that includes the aforementioned jig with the measurement sonar sensor platform together with the other components that have been used for conducting the experiments. Panel b shows the assembled system setup mounted on the P3DX robot.

based solely on ultrasound echolocation. Our measurement platform therefore generates ultrasonic logarithmic frequency sweep emissions ranging from $45\,\mathrm{kHz}$ down to $20\,\mathrm{kHz}$ that have been windowed with a Blackman window function [21] in order to reduce transients when emitting. These waveforms are comparable to what lesser spear-nosed bats (*Phyllostomus elongatus*) [22] or Daubenton's bats (*Myotis daubentonii*) [23] emit while echolocating. While these signals differ from the vocalizations emitted by *Micronycteris microtis* during gleaning behavior, we believe that the utilized pulses are applicable in our experimental setup. The reason for this is twofold: we scaled the 3D-printed pinnae of the *Micronycteris microtis* by a factor of 1.7 to adjust for the frequency response of the emitter and microphones, as the *Micronycteris microtis* typically uses very high frequencies up to $150\,\mathrm{kHz}$. On the other hand, *Micronycteris microtis* typically uses ultra short pulses with low-energy content ($200\,\mu\mathrm{s}$) in dense vegetation, which is probably for the reduction of reverberation. Figure 5a shows the time-domain representation of the emitted ultrasonic signal recorded using a Brüel & Kjær microphone in the far field whereas Figure 5b shows the spectrogram. Besides harmonics we can clearly distinguish our programmed frequency sweep from $45\,\mathrm{kHz}$ down to $20\,\mathrm{kHz}$. On the receiver side, the two microphones, embedded in the 3D-printed replica of the common big-eared bat ears, will capture these emissions. Due to the shape and orientation of the pinnae, the received echoes will exhibit spectral differences between the left and right ear with respect to the angle of incidence $\vec{\psi_k}$. This morphology-induced spatial filtering serves as a key cue in echolocation which is elaborated in [5], [6], [24]. Using bio-inspired pinnae also contributes to the low-cost attribute of this sensor since it implicitly adds target localization capabilities without the need of a microphone array and beamforming techniques [25]. The choise of using pinnae of the *Micronycteris microtis* for this system setup and experiment however could have differed since these techniques are also applicable to other bat pinnae [3], [4], [26]. To characterize the effect of the pinnae on the received ultrasonic emissions

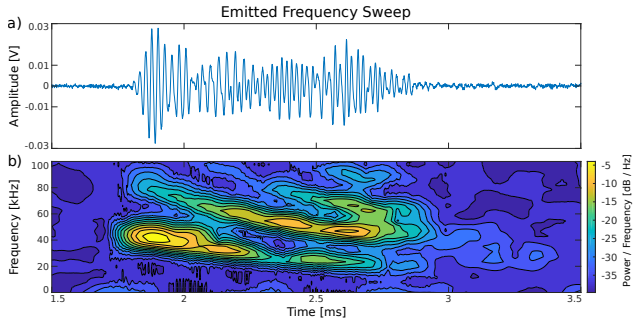


Fig. 5. Panel a) the time domain representation of the Polaroid transducer transmission of a logarithmic frequency sweep ranging from 45 kHz down to 20 kHz which was recorded with a Brüel & Kjær microphone recorded in the far field. Whereas b) shows the spectrogram representation of that same recorded output signal.

we have measured these impulse responses for a large part of the frontal hemisphere and thus created an Echo-Related Transfer Function (ERTF) [27]:

$$H^i_{\vec{\psi_k}}(\omega) = \mathcal{F}(h^i_{\vec{\psi_k}}(t))$$
$$\vec{\psi_k} = [\theta, \phi]$$

where $H^i_{\vec{\psi_k}}(\omega)$ is the transfer function of the microphone/ear with index $i \in \{\mathrm{L}, \mathrm{R}\}$ representing either the left and right microphone/ear, with $\mathcal{F}$ the Fourier transform and $h^i_{\vec{\psi_k}}(t)$ its equivalent impulse response. The vector $\vec{\psi_k}$ is used to describe the incident angle of the reflection using the azimuth $\theta$ and elevation $\phi$ relative to the bat pinnae. Figure 6 shows the ERTF plotted for four frequencies. These measurements of the frontal hemisphere range from $-90°$ to $+90°$ in azimuth angle and $-47°$ to $+30°$ in elevation angle. This asymmetrical elevation measurement is accounted by the range constraint of the used pan/tilt system.

Assuming the received emission in either microphone is a linear sum of every reflection delayed in time over an amount $\Delta t$ according to its traveled distance in combination with the speed of sound $v_s$, we can derive the microphone signals $s^L_m(t)$ and $s^R_m(t)$ as:

$$s^i_m(t) = \sum_{k=1}^{K} a_k \cdot h^i_{\vec{\psi_k}}(t) * s_b(t - \Delta t_k)$$
$$\Delta t_k = \frac{r_k \cdot 2}{V_s}$$

with index $K$ being the total number of reflections, $a_k$ the attenuation due to the traveled distance, $s_b(t)$ the pre-recorded base echo signal and $r_k$ the range of the $k^{th}$ reflection. The speed of sound in air $V_s$ is approximated to be $343\,\mathrm{m/s}$.

When the sensor platform is rotated, and consequently the pinnae are rotated with respect to the reflector(s), the inter-aural differences will be larger. This trait is advantageous and desirable for our control architecture, and plays an important role in biological sound localization [28], since these differences enable our system to differentiate reflectors on its path and to act upon that.

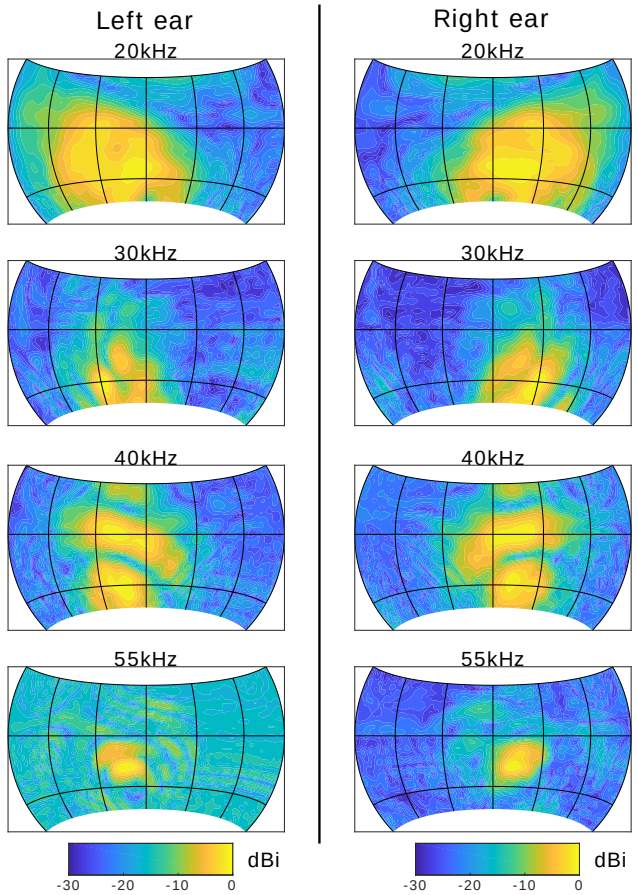


Fig. 6. Measured Echo-Related Transfer Function (ERTF) of the common big-eared bat. The ERTF is a collection of directivity patterns for a set of frequencies. These directivity patterns for these frequencies have been plotted using Lambert azimuthal equal area projections with a gridline spacing of 30°. These directivity patterns exhibit moving main lobes and notches, which have been shown to provide a high amount of information on the reflector's location [24].

Using the received microphone signals $s^i_m(t)$, where index $i$ represents either the left or the right microphone, in combination with cross-correlation techniques we can determine the time-of-arrivals of the reflected ultrasonic emissions for every microphone signal $s^i_m(t)$. The matched filter function uses a pre-recorded base echo signal $s_b(t)$, which was extracted from a previous measurement, together with the actual microphone signals $s^i_m(t)$:

$$s^i_r(t) = \mathcal{F}^{-1}\left\{S^i_m(\omega) \cdot S^*_b(\omega)\right\}$$

with $s^i_r(t)$ the resulting signal of the matched filter function with index $i$ as the used microphone signal, $S^i_m(\omega)$ the Fourier transformation of either microphone signal $s^i_m(t)$ and $S_b(\omega)$ the Fourier transformation of the pre-recorded base signal $s_b(t)$. When inspecting $s^i_r(t)$, the resulting waveform will display peaks which indicate the time delay of the reflected ultrasonic emissions. These peaks in the output signal of the matched filter therefore gives us an indication of reflectors in the horizontal plane. Using the speed of sound in air $V_s$, this can be correlated to a distance the reflector (or object) has to our measurement system. However when we

look into nature, this is not the approach that is used. Instead the cochlea of mammals forms a filter bank [29] to estimate the time-frequency distribution which enables echolocation. A biomimetic and computationally effective approach to this mammalian function is calculating the envelope function of the matched filter waveform $s_r^i(t)$. The envelope $s_{env}^i(t)$, of which the peaks can be used to estimate the range to an obstacle, is calculated using:

$$s_{env}^i(t) = h_{LPF}(t) * |s_r^i(t)|$$

where $h_{LPF}(t)$ is the impulse response of a low-pass filter where the cutoff frequency $f_c$ was chosen at $2\,\mathrm{kHz}$ which is convolved with the absolute value of $s_r^i(t)$ resulting in $s_{env}^i(t)$ being the envelope of our matched filtered waveform. These envelopes are used to estimate the amount of energy that was received in the left and right ear, $E^L$ and $E^R$ over the duration of the measurement $T$:

$$E^i = \sqrt{\frac{1}{T}\int_0^T |s_{env}^i(t)|^2 \cdot dt}$$

## IV. Subsumption Control Architecture

Using the envelope of the received and matched filtered microphone signals $s_{env}^i(t)$ in combination with the amount of energy received in the left $E^L$ and right ear $E^R$ we can determine what action or behavior should be exhibited by the autonomous robot. This approach to reactive control is similar to the work of Srinivasan et al. [30]–[32] where our approach makes use of echolocation instead of vision. In order to do this a behavior-based control architecture or subsumption control architecture was designed. This layered control system distinguishes itself by coupling these layers to a specific set of actions and priorities [9], [12]. This also means that only one layer, and hence behavior, will take control of the robot's action at a single measurement. Our implementation has only three layers or behaviors: collision avoidance, obstacle avoidance and straight driving. A fourth behavior, corridor following, based on the principle of optic or acoustic flow [33] that is present in both insect and mammal behavior, could have been implemented as well but has intentionally been left out of our scope since this is mostly relevant in corridor-like environments.

Which behavior will be chosen is dependent solely on the envelope signals $s_{env}^i(t)$ whereas the actions that are taken when a certain behavior is determined comes down to adjusting the linear velocity $V_l$ and the angular velocity $V_a$. In this setup these actions are executed as commands to ROS which in turn will translate these into motor commands.

*1) Collision Avoidance:* Collision avoidance is activated whenever the robot comes too close to a reflector. The invoked action would be to rotate until the driving path is free from collisions. This behavior is implemented to be ballistic, meaning that this behavior will persevere until there are no more reflections in its path. It is activated whenever the sum of the first part of $s_{env}^i(t)$, containing the early reflections in the space in front of the robot, and therefore indicating close by objects, is greater than a set threshold. The range of this first part is set relative to the size of the robot and the location of the sensor, which in this case was set to approximately $60\,\mathrm{cm}$. The rotating action or angular velocity $V_a$ is set to a fixed rotation $\alpha$, for this experiment $0.3\,\mathrm{rad/s}$. The sign of the angular velocity $\alpha$ is determined by the amount of energy that was received by the left and right ear up to the predefined range. Since the robot should avoid a collision with the perceived reflection, the linear velocity $V_l$ is set to zero.

$$V_l = 0 \qquad\qquad V_a = \pm\alpha$$

*2) Obstacle Avoidance:* Whenever the sum of signal $s_{env}^i(t)$ in a range between the $60\,\mathrm{cm}$ and $1.65\,\mathrm{m}$ is greater than the predefined threshold the obstacle avoidance behavior will be displayed. This behavior should steer the robot away from the closest reflector based on the difference between $E^L$ and $E^R$. In order to establish this behavior, the linear velocity $V_l$ is set at a fixed level $V_l^m$, which was set to $0.2\,\mathrm{m/s}$, while the angular velocity $V_a$ is set at a fixed level of $0.02\,\mathrm{rad/s}$ multiplied with a normalized energy difference [5].

$$V_l = V_l^m \qquad\qquad V_a = 0.02 \cdot \frac{(E^R - E^L)}{1000}$$

*3) Straight Drive:* When neither of these two behaviors are chosen the robot returns to its most basic behavior, i.e. driving straight. This behavior comes down to a linear velocity $V_l$ that is fixed to $V_l^m$ and an angular velocity of zero.

$$V_l = V_l^m \qquad\qquad V_a = 0$$

## V. EXPERIMENTAL RESULTS

Using the aforementioned experimental setup with the P3DX two-wheeled robot equipped with an Intel NUC and our sonar sensor measurement platform we have conducted autonomous navigation experiments in an unknown office environment in which we have placed a number of obstacles together with a number of cubicle wall panels to create artificial protruding wall segments. In order to capture the ground truth data for this environment and afterwards track the path of the robot during our autonomous driving, ROS was used toghether with the Hokuyo LIDAR. The results of one of these experiments is shown in Figure 7 that shows the pre-recorded ground truth map on which the trajectory is plotted. Solely the proposed sonar sensor is used to determine the behavior of the P3DX robot. The determined behavior for a location on the trajectory is represented by a colored circle for which red is straight drive, green is obstacle avoidance and blue is collision avoidance.

## VI. DISCUSSION AND FUTURE WORK

The results of our autonomous navigation in cluttered unknown environments proved to be very successful, since no collisions occurred and the trajectory remained fairly stable. We believe this flexible and low-cost sonar sensing platform is a valuable addition to the already vast collection of sensor modalities that exist within robotics. Due to the compact form-factor, flexibility and high level of integration

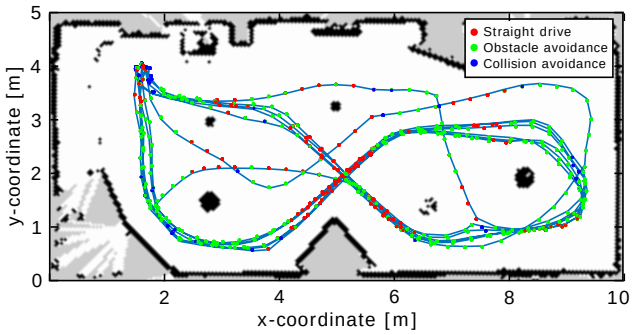


Fig. 7. The figure above shows recorded ground truth of the cluttered environment and trajectory of the P3DX robot using the LIDAR. This sensor was only used for this purpose since the actual autonomous behavior of the robot was determined by the measurements of our proposed sonar sensing platform. The colored dots on the trajectory indicate what type of behavior was chosen where red is straight drive, green is obstacle avoidance and blue is collision avoidance.

of our proposed acoustic sensing platform, it can be easily used to conduct other echolocation experiments. This could also prove to become a useful tool in synthetic psychology and biomimetic robots [31], [34] which would demonstrate the powerful interaction between a subsumption architecture and advanced sensing modalities.

In future experiments we will use this sonar sensor platform and control architecture for other types of autonomous vehicles and other applications. An increasingly popular vehicle that has attracted great attention, ranging from hobbyist to research, are drones. This type of UAVs would be very interesting to use for biomimetic bat research since this would enable us to mimic flight patterns based on the sonar data. This seemed unfeasible up until now since even recent other research [35] required large and powerful robots due to the considerable weight and size of the used (ultrasonic) equipment. Since our sonar sensor platform only measures $7.5\,\mathrm{cm} \mathrm{x} 5.0\,\mathrm{cm} \mathrm{x} 2.8\,\mathrm{cm}$ and weighs $90\,\mathrm{g}$, which includes the 3D-printed plastic parts, it could be feasible to mount this on a "standard" drone without hindering its flight dynamics or drastically reducing its flight time. Figure 8 illustrates that it is certainly possible to fit our sonar sensing platform on an ERLE-COPTER drone. Since this drone should support payloads up to $1\,\mathrm{kg}$, according to the documentation, it should be feasible to generate enough lift to fly with our sensor mounted on it. This can provide insights into 3D-flight algorithms using sonar, which is to the best of our knowledge the first sonar sensor platform that can make this possible.

An other application for our sonar sensor platform would be to combine this with a pan/tilt system thus enabling mimicking head movements of bats in biomimetic experiments that focus on modeling bat movements in view of prey capture [36].

Fig. 8. Image showing an ERLE-COPTER drone with a Raspberry Pi as its main processor unit. In the front, our sonar sensor platform easily fits on the enclosure. Since this drone should support payloads up to $1\,\mathrm{kg}$, according to the documentation, it should be feasible to generate enough lift to fly with our sonar sensor platform, which weighs only $90\,\mathrm{g}$, mounted on it.

## References


[1] R. Wehner, "Desert ant navigation: how miniature brains solve complex tasks," *Journal of Comparative Physiology A*, vol. 189, no. 8, pp. 579–588, aug 2003. [Online]. Available: https://doi.org/10.1007/s00359-003-0431-1

[2] M. Srinivasan, S. Zhang, M. Lehrer, and T. Collett, "Honeybee navigation en route to the goal: visual flight control and odometry," *Journal of Experimental Biology*, vol. 199, no. 1, pp. 237–244, 1996. [Online]. Available: http://jeb.biologists.org/content/199/1/237

[3] F. Schillebeeckx, F. De Mey, D. Vanderelst, and H. Peremans, "Biomimetic sonar: Binaural 3D localization using artificial bat pinnae," *International Journal of Robotics Research*, 2011.

[4] F. Schillebeeckx, F. De Mey, and H. Peremans, "Bio-inspired sonar antennae: Enhancing directivity patterns for localization," in *Proceedings of the 2nd Biennial IEEE/RAS-EMBS International Conference on Biomedical Robotics and Biomechatronics, BioRob 2008*, 2008.

[5] D. Vanderelst, M. W. Holderied, and H. Peremans, "Sensorimotor Model of Obstacle Avoidance in Echolocating Bats," *PLoS Computational Biology*, 2015.

[6] D. Vanderelst and H. Peremans, "A computational model of mapping in echolocating bats," *Animal Behaviour*, 2017.

[7] J. Steckel, A. Boen, and H. Peremans, "Broadband 3-D sonar system using a sparse array for indoor navigation," *IEEE Transactions on Robotics*, vol. 29, pp. 161–171, 2013.

[8] J. Steckel and H. Peremans, "BatSLAM: Simultaneous Localization and Mapping Using Biomimetic Sonar," *PLoS ONE*, 2013.

[9] ——, "Acoustic Flow-Based Control of a Mobile Platform Using a 3D Sonar Sensor," *IEEE Sensors Journal*, 2017.

[10] I. Geipel, K. Jung, and E. K. Kalko, "Perception of silent and motionless prey on vegetation by echolocation in the gleaning bat Micronycteris microtis," *Proceedings of the Royal Society B: Biological Sciences*, 2013.

[11] R. Arkin, "Behaviour-based robotics," 1998.

[12] R. A. Brooks, "A Robust Layered Control System For A Mobile Robot," *IEEE Journal on Robotics and Automation*, 1986.

[13] Adept Mobile Robots, "Pioneer 3-DX," p. 2, 2011.

[14] R. Kerstens, D. Laurijssen, W. Daems, and J. Steckel, "Widening the Directivity Patterns of Ultrasound Transducers Using 3-D-Printed Baffles," *IEEE Sensors Journal*, vol. 17, no. 5, pp. 1454–1462, mar 2017. [Online]. Available: http://ieeexplore.ieee.org/document/7792174/

[15] L. Hokuyo Automatics Co, "Scanning Laser Range Finder Documentation," *Hokuyo Automatic LTD*, pp. 1–5, 2005. [Online]. Available: http://www.hokuyo-aut.jp/02sensor/07scanner/download/products/urg-04lx/data/URG-04LX_spec_en.pdf

[16] M. Quigley, K. Conley, B. Gerkey, J. Faust, T. Foote, J. Leibs, R. Wheeler, and A. Y. Ng, "ROS: an open-source Robot Operating System," in *ICRA workshop on open source software*, vol. 3, no. 3.2. Kobe, Japan, 2009, p. 5.

[17] STMicroelectronics, "Overview STM32F427xx STM32F429xx

advanced ARM-based 32-bit MCUs," 2018. [Online]. Available: http://www.st.com/resource/en/datasheet/stm32f429zi.pdf
[18] Knowles Electronics, "FG-23329-P07 Knowles.pdf," p. 2, 2005.
[19] Senscomp, "Series 7000 Ultrasonic Sensor Features :," pp. 1–3, 2014.
[20] Future Technology Devices International and Ltd, "FT4232H Quad High Speed USB to Multipurpose UART/MPSSE IC," pp. 1–44, 2010.
[21] A. V. Oppenheim, *Discrete-time signal processing*. Pearson Education India, 1999.
[22] W. Bogdanowicz, R. D. Csada, and M. B. Fenton, "Structure of noseleaf, echolocation, and foraging behavior in the Phyllostomidae (Chiroptera)," *Journal of Mammalogy*, vol. 78, no. 3, pp. 942–953, 1997.
[23] A. R. Britton and G. Jones, "Echolocation behaviour and prey-capture success in foraging bats: laboratory and field experiments on Myotis daubentonii," *Journal of Experimental Biology*, vol. 202, no. 13, pp. 1793–1801, 1999. [Online]. Available: http://jeb.biologists.org/content/202/13/1793
[24] D. Vanderelst, J. Reijniers, J. Steckel, and H. Peremans, "Information generated by the moving pinnae of Rhinolophus rouxi: tuning of the morphology at different harmonics." *PloS one*, vol. 6, no. 6, p. e20627, jan 2011. [Online]. Available: http://dx.plos.org/10.1371/journal.pone.0020627
[25] J. Steckel, F. Schillebeeckx, and H. Peremans, "Biomimetic sonar, outer ears versus arrays," in *SENSORS, 2011 IEEE*, oct 2011, pp. 821–824.
[26] F. Schillebeeckx, "Bio-Inspired In-Air Sonar Localization: What Artificial Pinnae do for Robotic Bats," Ph.D. dissertation, Universiteit Antwerpen (Belgium, 2011.
[27] J. Steckel and H. Peremans, "Biomimetic sonar for biomimetic SLAM," in *2012 IEEE Sensors*. IEEE, oct 2012, pp. 1–4.
[28] B. Grothe, M. Pecka, and D. McAlpine, "Mechanisms of Sound Localization in Mammals," *Physiological Reviews*, vol. 90, no. 3, pp. 983–1012, 2010. [Online]. Available: https://doi.org/10.1152/physrev.00026.2009
[29] L. Robles and M. A. Ruggero, "Mechanics of the Mammalian Cochlea," *Physiological Reviews*, vol. 81, no. 3, pp. 1305–1352, 2001. [Online]. Available: https://doi.org/10.1152/physrev.2001.81.3.1305
[30] M. V. Srinivasan, "Visual control of navigation in insects and its relevance for robotics," *Current Opinion in Neurobiology*, vol. 21, no. 4, pp. 535–543, 2011. [Online]. Available: http://www.sciencedirect.com/science/article/pii/S0959438811000882
[31] K. Weber, S. Venkatesh, and M. V. Srinivasan, "Insect inspired behaviours for the autonomous control of mobile robots," in *Proceedings - International Conference on Pattern Recognition*, 1996.
[32] R. Strydom, S. Thurrowgood, and M. V. Srinivasan, "Visual odometry: Autonomous UAV navigation using optic flow and stereo," in *Australasian Conference on Robotics and Automation, ACRA*, 2014.
[33] R. Müller and H.-U. Schnitzler, "Acoustic flow perception in cf-bats: Properties of the available cues," *The Journal of the Acoustical Society of America*, vol. 105, no. 5, pp. 2958–2966, 1999. [Online]. Available: https://doi.org/10.1121/1.426909
[34] D. Floreano, M. V. Srinivasan, J. C. Zufferey, and C. Ellington, *Flying insects and robots*, 2010.
[35] I. Eliakim, Z. Cohen, G. Kosa, and Y. Yovel, "A fully autonomous terrestrial bat-like acoustic robot," *PLOS Computational Biology*, vol. 14, no. 9, pp. 1–13, 2018. [Online]. Available: https://doi.org/10.1371/journal.pcbi.1006406
[36] D. Vanderelst and H. Peremans, "Modeling bat prey capture in echolocating bats: The feasibility of reactive pursuit," *Journal of Theoretical Biology*, vol. 456, pp. 305–314, 2018. [Online]. Available: http://www.sciencedirect.com/science/article/pii/S0022519318303515